Japanese Journal of Applied Physics
Vol. 46, No. 10A, 2007, pp. 6626–6633

Signal Enhancement and Limiting Factors in Waveguides Containing Si Nanoclusters and Er^{3+} Ions

Daniel NAVARRO-URRIOS*, Nicola DALDOSSO, Cristina GARCÍA[1], Paolo PELLEGRINO[1], Blas GARRIDO[1], Fabrice GOURBILLEAU[2], Richard RIZK[2], and Lorenzo PAVESI

Laboratorio Nanoscienze, Dipartimento di Fisica, Università di Trento, Via Sommarive 14, I-38050 Povo (Trento), Italy
[1]*EME-Departament d'Electrònica, Universitat de Barcelona, Martí i Franquès, 1, 08028 Barcelona, Spain*
[2]*SIFCOM, UMR CNRS 6176, ENSICAEN, 6 Boulevard Maréchal Juin, 14050 Caen, France*

(Received January 8, 2007; accepted July 9, 2007; published online October 9, 2007)

Rib-loaded waveguides containing Er^{3+} ions coupled to Si nanoclusters (Si-nc) prepared by reactive magnetron co-sputtering have been studied with the aim of improving the optical amplification at 1.54 μm. A set of waveguides with different refractive indices has been fabricated by reducing the annealing duration to investigate the influence of the reorganization (quality) of the dielectric matrix and of the Si-nc clustering on the amplification of Er^{3+} signal. Insertion losses, photoluminescence, lifetime and pump/probe measurements have been carried out to characterize, understand and optimize the main factors that are preventing a net optical gain in these samples, i.e., low excitable erbium fraction through the nanoclusters, cooperative up-conversion and confined carrier absorption. Evidences of partial inversion of the Er^{3+} ions excited via Si-nc are presented. [DOI: 10.1143/JJAP.46.6626]

KEYWORDS: silicon nanocluster, erbium, optical amplifier, waveguides, silicon photonics

1. Introduction

Integrated erbium-doped waveguide amplifiers (EDWAs) are fundamental elements in planar lightwave circuits thank to their compactness and easy of integration on Silicon wafers. A limitation to their diffusion is their cost. One way to overcome the cost is the use of broadband efficient sensitizers for Er^{3+} ions such as Si nanoclusters (Si-nc) in SiO_2 which allows substituting expensive pump sources by low cost broad-band excitation lamps. In fact, the pump light is absorbed by the Si-nc which transfer their excitation to the Er^{3+} ions. Thus, the effective excitation cross section of the Er^{3+} 1.54 μm luminescence (σ_{exc}) broadens and strengthens up to values of 10^{-16} cm^2, when visible light is used and at low flux.[1–5] These σ_{exc} values are orders of magnitude larger than those of Er^{3+} in SiO_2, where one measures absorption cross section values of 10^{-21} cm^2 at $\lambda_{exc} = 980$ nm.[6,7] Quantum efficiencies greater than 60% and Si-nc to Er^{3+} transfer rates higher than 1 μs^{-1} by pumping at 488 nm have been also measured.[8] In addition to the increase of σ_{exc}, Si-nc increase the average refractive index of the dielectrics, allowing good light confinement, and conduct electrical current,[9,10] which opens the route to electrically pumped optical amplifiers. Encouraging results about Er^{3+} coupled Si-nc optical amplifiers have been reported by Shin *et al.*[11,12] and by us.[13]

In order to engineer the system, with the aim of achieving a net optical gain in the amplifiers, the role of detrimental processes is to be figured out. Indeed, it is likely that processes like cooperative up-conversion (related to the Er content), confined carrier absorption (CA), Auger non radiative de-excitations and excited state absorption (ESA) within the Si-nc prevent net optical gain when reaching high pumping fluxes.[13–15] While in our reactive magnetron co-sputtering prepared samples we have experimental evidences of the presence of the two first processes (cooperative up-conversion and CA), we have not detected measurable fingerprints of the latter ones. In this manuscript we quantify the importance of the two first mechanisms as a function of the annealing time, having fixed the other processing parameters.

The Er content in the active layer of the waveguide amplifier should be high enough to have large gain still remaining below a threshold value to prevent the occurrence of clustering and cooperative up-conversion phenomena.[15–17] Er^{3+} concentrations not exceeding $(2–4) \times 10^{20}$ cm^{-3} are suggested.[18,19] In addition, the Si-nc densities and sizes have to be tuned to achieve a high rate of coupling with Er^{3+} ions to excite them efficiently, together with low propagation losses and negligible confined carrier absorption in the waveguide. However, the energy transfer mechanism from Si-nc to Er^{3+} is still far from being completely understood.[20] In this work quite low values of Si-nc density [$(1–5) \times 10^{17}$ cm^{-3}] in comparison to the Er^{3+} content have been achieved. Consequently, only a small percentage of the erbium population (2–3%) is sensitive to be excited through indirect energy transfer from the excited Si-nc. This fact, although detrimental for the performance of the amplifier, has allowed us to have some insights in the dependence of the coupling constant with the distance of Er^{3+} from Si-nc. The experimental consequence of such a behavior is an effective excitation cross section that depends on the photon flux. In this work, we also address this issue for different annealing times.

To complete the study we show in the last part of the manuscript a study of the amplification properties of this set of samples. Positive signal enhancement has been measured; whose values are consistent with what expected from the previous optical characterization. Therefore, although only an inversion factor of about 10% has been achieved for the highest pump fluxes used, most of the enhancement comes from directly excited erbium. A further increase of the Silicon content to increase the Si-nc density by using low annealing times is suggested in order to minimize the power threshold needed to obtain full population inversion.

2. Waveguide Fabrication and Experimental Details

Er^{3+} doped Si-nc silica waveguides have been prepared

*E-mail address: navarro@science.unitn.it

Table I. Sample parameters: annealing time, Si-excess, Er content, refractive index n at 632.8 nm, fundamental optical mode confinement factor Γ.

Sample	Annealing time (min)	Si excess (at. %)	Er content ($\times 10^{20}$ cm^{-3})	n	Γ
B	60	7	4 ± 0.1	1.545	0.51 ± 0.02
C	30	6–7	5.4 ± 0.2	1.516	0.48 ± 0.02
D	10	6–7	5.4 ± 0.2	1.48 ± 0.01	0.28 ± 0.03

by a multi-wafers reactive magnetron co-sputtering of a pure silica target topped with Er_2O_3 pellets. The incorporation of Si excess in the film was obtained by mixing the plasma with hydrogen, owing to its ability to reduce the oxygen provided by the silica target. The hydrogen rate (mixed to argon) was kept to 60% while the Si substrates, on which a 15 μm thermal SiO_2 layer was previously thermally grown, were not intentionally heated. More details on the process can be found elsewhere.[18] After the deposition of about 1 μm thick Er/silicon rich oxide (SRO) layer, a 1 μm thick SiO_2 cladding layer has been deposited by sputtering a SiO_2 target in pure argon plasma. Then the wafers have been annealed, for different times at 900 °C under pure N_2 flux to activate Er^{3+} ions, to induce the precipitation of the Si excess into nanoclusters that are expected to play the role of sensitizers of Er^{3+} ions. The annealing temperature was chosen on the basis of previous optimization studies.[18,19] The annealing duration has been varied between 1 and 240 min: annealing times longer than 60 min have shown no improvement in the optical properties of Er^{3+} doped Si-nc systems. This annealing time variation aimed at controlling the Si-nc size. Secondary ion mass spectroscopy (SIMS) and Rutherford backscattering spectroscopy (RBS) have been performed to determine Si and Er content (see Table I). It is worth noting that the total Si excess is roughly the same for all the samples.

Optical lithography and reactive ion etching have been used to define 2–3 cm long rib-loaded waveguides with rib widths ranging between 3.5 to 12 μm. It is worth noting here that the very low refractive indices of the 5 and 1 min annealed films result in no light confinement in the 1500–1600 nm range. On the contrary, waveguides annealed at 60 min (from now on sample B), 30 min (sample C), and 10 min (sample D) have quite good light confinement: calculated optical confinement factors Γ of the fundamental mode at 1535 nm are 0.51, 0.48, and 0.28, respectively.

The optical confinement factors have been deduced from the layer thickness and the material refractive index measured by using the m-line technique[21] at 633 nm. These measurements allow also figuring out the Si-nc size as a function of the annealing time. The index of refraction n of the Si-nc rich oxide layer has an intermediate value between that of Si and that of the surrounding dielectric. A simple estimate of the effective material refractive index can be obtained by the Bruggeman effective medium theory by considering that the film is composed by amorphous Si-nc (annealing at 900 °C is not enough to induce crystallization[5]) embedded into a matrix of sub-stoichiometric defected silica SiO_x (with x varying between 1.63 and 2 with increasing the annealing time). The detailed analysis of this study can be found elsewhere.[22] It is worth noting here that the refractive index grows as a function of the annealing time (see Table I). From the quantitative analysis we concluded that the substoichiometric matrix becomes close to stoichiometric by increasing the annealing time, precipitating the excess Si into the nanoclusters. Fitting the measured refractive index with the Bruggeman model, the excess Si fraction which precipitates into the Si-nc and the x of the sub-stoichiometric silica can be inferred. From energy filtered transmission electron microscopy (EFTEM) studies,[23] a Si-nc density of $(1–5) \times 10^{17}$ cm^{-3} can be estimated for all the samples. Combining this value with the total Si excess that has been precipitated into Si-nc for each annealing time we can estimate the average size of the Si-nc. The results of these estimates are shown in Fig. 1, where it is clear that Si-nc size grows with increasing the Si excess forming Si-nc, i.e., increasing the annealing time. In sample D, for example, the analysis of the Si-nc size distribution determined from the EFTEM images (inset of Fig. 1) shows that the mean radius for this sample is 1.6 ± 0.3 nm, which is actually compatible with the value obtained with our model.

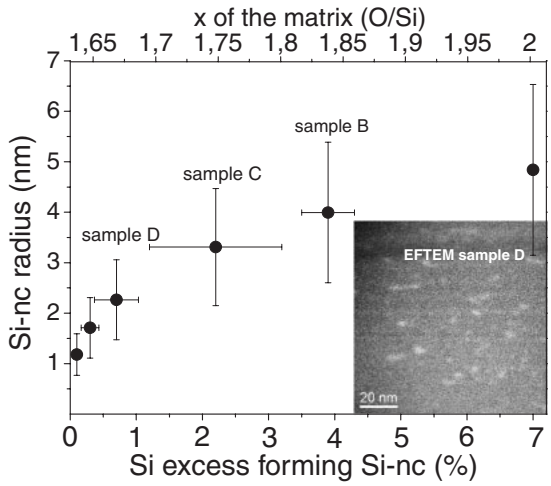

Fig. 1. Radius of Si-nc vs the silicon excess forming Si-nc and TEM micrograph of one of the samples (inset).

Photoluminescence measurements have been performed by pumping with the 476 nm (out of Er^{3+} resonance pumping conditions) and 488 nm (resonance pumping conditions) lines of an Argon laser and detecting light with a monochromator coupled to an InGaAs photomultiplier. Lifetime measurements were performed using a Ge detector cooled with liquid nitrogen. The laser beam was chopped at 15 Hz and its power density was ranging from 5 to 450 mW cm^{-2}. The overall time response of the experimental setup is about 0.5 ms.

Internal gain measurements of the rib-loaded waveguides have been performed by butt-coupling signal light through a single-mode polarization-preserving tapered fiber moved by a piezo-electric stage. The light exiting the end facet of the waveguide was observed with a microscope objective matched, through a prism beam splitter, both to a zoom mounted on an InGaAs camera and to a Ge detector. We have used two different signal light sources: a tunable laser (1.5–1.6 μm) that cover the $^4I_{13/2} \rightarrow {}^4I_{15/2}$ internal Er^{3+}

transition (peaked at 1535 nm) and a diode laser operating at 1310 nm, well away from transitions related to Er^{3+} ions. The pump source was a Millenia laser (532 nm, 10 W) focused on the waveguide surface onto a stripe 100 μm wide and 1 cm long by means of a cylindrical lens. The alignment of the pump beam and the rib-loaded waveguide was checked by two cameras, which allow observing both the waveguide surface and exit facet. It has to be considered that the pumping wavelength is weakly coupled to an Er^{3+} absorption transitions (the absorption cross section at this wavelength is roughly 1/3 of that at 488 nm). Some measurements were done by using the 488 nm line of an Argon laser, resonant with an Er^{3+} absorption peak ($^4I_{15/2} \rightarrow {}^4F_{7/2}$). In order to eliminate the diffused light and the amplified spontaneous emission (ASE) the weak probe signal was chopped (10 kHz) and measured through a lock-in system.

3. Emission Cross Sections

The emission cross section σ_{em} of the $^4I_{13/2} \rightarrow {}^4I_{15/2}$ transition of the Er^{3+} ions is not significantly enhanced by the presence of the Si-nc and only small differences due to the variation of the effective refractive indices were observed.[24] Measuring the low pumping rate luminescence spectra, $\sigma_{em}(\nu)$ can be obtained in a quantitative manner by using one of the McCumber relations[26]

$$\sigma_{em}(\nu) = \sigma_{abs}(\nu) \exp\left(\frac{\varepsilon - h\nu}{kT}\right), \quad (1)$$

once $\sigma_{abs}(\nu)$, the absorption cross section, is known. In eq. (1), ε is the transition energy between the lowest levels of the two $^4I_{13/2}$ and $^4I_{15/2}$ manifolds, T the sample temperature, and k the Boltzmann constant.

$\sigma_{abs}(\nu)$ has been measured by the insertion loss technique.[13,27] Absorption losses (α_{abs}) of 7.5, 8.5, and 5.4 dB/cm for samples B, C, and D, respectively, have been measured at 1535 nm.[24] Then $\sigma_{abs}(\nu) = \alpha_{abs}(\nu)/\Gamma N_{Er}$, where N_{Er} is the Er^{3+} concentration.[28] From eq. (1), $\sigma_{em}(\nu)$ is obtained (Fig. 2). It is observed that decreasing the annealing time, $\sigma_{em}(\nu)$ narrows and strengthens, contrary to what expected due to the refractive index decrease since $\sigma_{em}(\nu)$ is roughly proportional to the refractive index.[29] Actually the emission cross section of sample D is almost twice that of sample B. These behaviors are mainly due to the evolution of the local Er^{3+} environment with the annealing duration which is changing from a defected SiO_x where small Si-nc clusters are present to a two phase Si-nc and SiO_2 system.[24] The influence of the local field on the erbium level structure is clearly evidenced when comparing the spectral shapes for the different samples. If only medium fields were involved, no spectral shape change will be observed. The longer the annealing time, the more erbium ions behave as in a pure silica glass (without Si-nc).

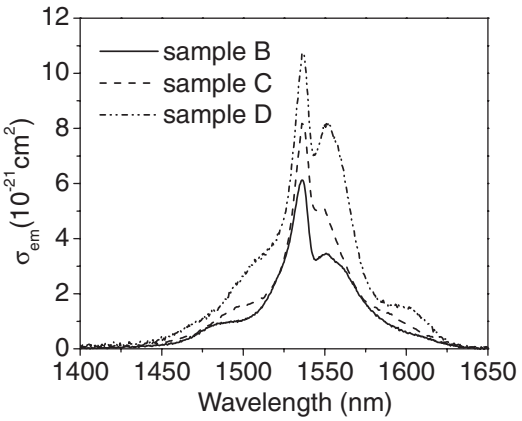

Fig. 2. Emission cross sections calculated from PL spectra at low pump power for samples B (solid line), C (dashed line), and D (dash and dots).

4. Lifetime Measurements

Luminescence decay measurements at 1535 nm have been performed as a function of the photon flux, Φ. The Er^{3+} lifetime at low photon flux increases with annealing time (from 1.9 ms for sample D to 3.8 ms for sample B) whereas σ_{em} decreases (Fig. 2). As already reported, the radiative lifetime increases when the annealing time increases,[24] but this effect is not enough to explain such a strong increase of the total lifetime. In fact, the probability of having non-radiative recombination increases with decreasing the annealing time for the three studied samples.[24] At low pump fluxes (10^{16}–10^{17} photons $cm^{-2}\,s^{-1}$) the temporal decay of the PL signal is well fitted by a single exponential law, which allows associating the behavior of the non-radiative lifetime to recombinations with defects or to concentration quenching effects between excited and non-excited Er^{3+} ions. It is worth noting that the probability of having this kind of recombinations is found to be independent of the excited Er^{3+} and of the pump photon flux. By increasing the pump flux, cooperative up-conversion recombination between close excited Er^{3+} ion pairs starts to play an important role among the other non-radiative recombination paths.

To figure out the role of the different de-excitation mechanism, we have modeled the photoluminescence decay by solving the differential equation that rules the decay rate of the excited level of the Er^{3+} population (N_2) taking into account specifically the cooperative up-conversion:

$$\frac{dN_2(t)}{dt} = -\frac{N_2(t)}{\tau_d} - C_{up}N_2(t)^2, \quad (2)$$

where τ_d is the lifetime, which counts for the radiative and the N_2 independent non-radiative recombination paths, and C_{up} is the up-conversion coefficient between pairs of excited ions.

Aiming at extracting these last two parameters it is necessary to know the initial excited state population for each pump photon flux. Thus, quantitative measurements of the photon flux emitted from the samples were performed by using a reference sample whose emission has been independently evaluated and quantified.[23] It is so possible to correlate the number of emitted photons to the population of the excited level.

In Fig. 3, the temporal dependence of N_2 for the various samples is reported starting from the steady state population generated at a pump photon flux of 1×10^{20} photons $cm^{-2}\,s^{-1}$. We have been able to fit the set of experimental N_2 decays obtained for different pump fluxes by using eq. (2) with fixed values τ_d and C_{up}. The extracted parameters are shown in the inset of Fig. 3: up-conversion is quite strong in sample D, weak in sample C and even weaker in sample B. We think that this decreasing of the

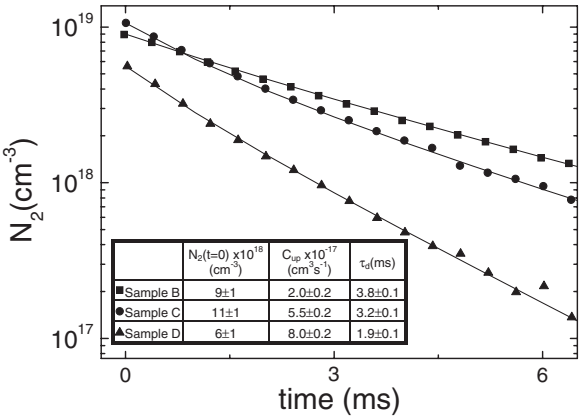

Fig. 3. Temporal behavior of the excited state Er^{3+} population N_2, starting from the steady population obtained at a photon flux of 10^{20} photon $cm^{-2}\,s^{-1}$. With this photon flux the decays are no more pure exponential due to cooperative up-conversion. The inset shows the parameters extracted from the fitting of the experimental data.

cooperative up-conversion strength is related with the improvement of the matrix when increasing the annealing time.

5. Effective Excitation Cross Sections

From time resolved luminescence measurements it is also possible to extract the effective excitation cross section, σ_{exc}, of the Er^{3+} ions. In fact, for low pump photon flux, $\Phi \sim 10^{16}$–10^{17} photons $cm^{-2}\,s^{-1}$, the difference between the reciprocals of the luminescence rise time (τ_r) and decay time (τ_d) can be expressed by:[7)]

$$\frac{1}{\tau_r} - \frac{1}{\tau_d} = \sigma_{exc}\Phi, \tag{3}$$

Figure 4 reports the left part of eq. (3) as a function of the pump photon flux Φ for samples B, C, and D excited by resonant (488 nm) and non-resonant (476 nm) wavelengths. A single σ_{exc} value is not able to fit the data. If we want to keep the simple (3), we have to divide the data in two Φ regions and use two different σ_{exc} values for $\Phi \approx 10^{16}$ to 10^{17} and 10^{17} to 10^{18} photons $cm^{-2}\,s^{-1}$. The results of the fits are reported in Fig. 4. We observe that:

i) for all the samples, σ_{exc} are orders of magnitude higher than those typical of Er^{3+} in pure silica ($\sim 10^{-21}$ cm^2), which is a consequence of the Er^{3+} excitation via the Si-nc;
ii) the slope is changing with increasing pump photon flux Φ, which means that σ_{exc} depends on Φ. This effect will be discussed in the following;
iii) for samples B and C, resonant (488 nm) and non-resonant (476 nm) excitation wavelengths result in the same σ_{exc}, strongly supporting the sensitizing action of the Si-nc;
iv) however, σ_{exc} of sample D is surprisingly higher with resonant pumping. Note that the values are higher than those for direct Er^{3+} absorption. Similar data were reported in ref. 31 without explanation. Since Si-nc absorption smoothly increases as the wavelength decreases,[30)] at the moment we miss the explanation. The very short annealing time could be involved, since the matrix is rich in defects which could prevent or affect the energy transfer from the Si-nc.

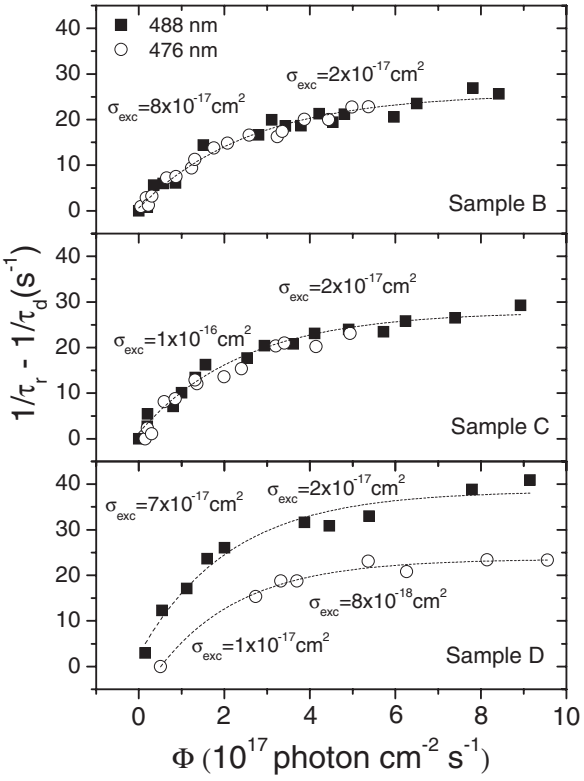

Fig. 4. Difference between the reciprocals of the rise (τ_r) and decay (τ_d) time at low pump flux for 488 nm (solid squares) and 476 nm (empty circles) pumping. The slopes of the curves give σ_{exc}.

Let us try to explain and model the apparent decrease of the effective σ_{exc} with Φ. In order to find the more appropriate model we have fitted with the same set of equations and parameters both the lifetime data as a function of the flux for low pump photon fluxes (Fig. 4, top panel) and the excited Er^{3+} population obtained from PL measurements for higher fluxes (Fig. 5, open circles). We focus on the results of sample B for the sake of clearness. The model should be able to explain the results of these two different measurements at two completely different pump flux regimes.

Let us briefly describe the model. The exciton population within the Si-nc generated by the pump light can be expressed by the following rate equation:

$$\frac{dN_{Si}^*}{dt} = \sigma_{Si}\Phi(N_{Si} - N_{Si}^*) - \frac{N_{Si}^*}{\tau_{Si}} - k_t N_{Si}^* C_{ind} N_{Er}, \tag{4}$$

where N_{Si}^* is the density of excitons, N_{Si} is the total density of Si-nc and σ_{Si} is the absorption cross section of the Si-nc at the pumping wavelength. Note also that τ_{Si} is the intrinsic lifetime of the exciton that is a combination of radiative and non-radiative contributions. k_t is the average coupling rate of the fraction C_{ind} of Er^{3+} ions coupled to Si-nc, i.e., we assume that, of the total Er^{3+} content N_{Er}, only a density $C_{ind}N_{Er}$ is coupled to the Si-nc. It can be argued that within our experimental conditions ($\Phi \ll 10^{20}$ photons $cm^{-2}\,s^{-1}$ for the excitation cross section measurement), the excitation transfer from Si-nc to Er^{3+} is the dominant deexcitation path and, thus, the steady state solution of eq. (4) is:

$$N_{Si}^* = \frac{\sigma_{Si}\Phi N_{Si}}{k_t C_{ind} N_{Er}}. \tag{5}$$

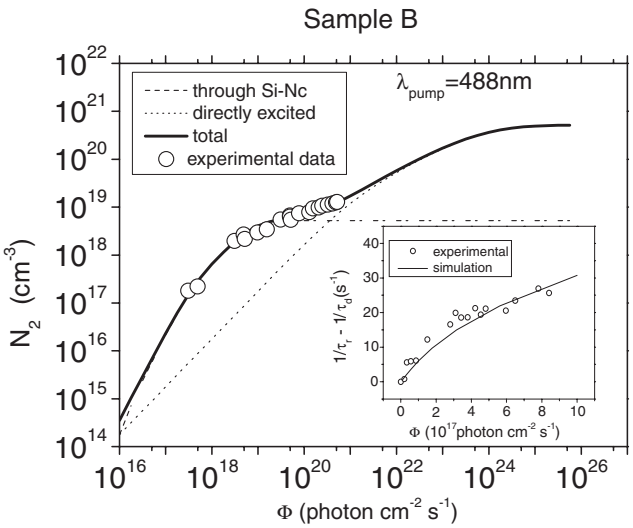

Fig. 5. Sample B: total excited Er^{3+} population as a function of pump photon flux as measured (empty circles) and simulated (solid line). The simulated curve is the sum of the directly excited Er^{3+} (dotted line) and Er^{3+} excited through Si-nc (dashed line). The inset shows the simulated and experimental curves of the difference between the reciprocals of the rise (τ_r) and decay (τ_d) times at low pump flux. The following parameters have been used in the simulations: $\tau_d = 3.8$ ms, $C_{up} = 2 \times 10^{-17}$ cm^3 s^{-1}, $R_0 = 0.5$ nm, $\sigma_0 = 3 \times 10^{-16}$ cm^2, $\sigma_d = 5 \times 10^{-21}$ cm^2, $R_{nc} = 4$ nm.

As for the Er^{3+} ions, we assume a two level system to model the rate equations. In fact, other processes that involve higher energy levels are assumed to relax so fast to the second excited level that we can consider the ion as an effective two level system. Auger back transfer to the Si-nc has also been neglected, as it is not a strong recombination path in our material.[32] We have considered that the equilibrium situation is reached much faster for the exciton population than for the population of the different energy levels of Er^{3+}, which means that we can neglect the lifetime of the exciton when it is compared with the lifetime of the $^4I_{13/2}$ state of Er^{3+}. While only a fraction $C_{ind}N_{Er}$ can be excited through the nanoclusters, the whole Er^{3+} population is susceptible to be excited by direct photon absorption, being their excitation cross section σ_d. Moreover, cooperative up-conversion is considered and excited state absorption neglected. Therefore, within our assumptions, the rate equation for the excited level of the Er^{3+} ions reduces to:

$$\begin{aligned}\frac{dN_2}{dt} &= KN_{Si}^{*}N_1 + \sigma_d\phi N_1 - \frac{N_2}{\tau_d} - C_{up}N_2^2 \\ &= \sigma_{exc}\phi N_1 - \frac{N_2}{\tau_d} - C_{up}N_2^2,\end{aligned} \tag{6}$$

where N_1 is the density of Er^{3+} in the ground state, $N_{Er} = N_1 + N_2$. Note that the coupling between the Er^{3+} ions and the Si-nc is here described by a coupling rate K which depends on the particular Er^{3+} ion considered, thus k_t used in eq. (4) is an average of the various K over the Er^{3+} ion coupled population. In eq. (6), we have introduced the effective excitation cross section σ_{exc} as:

$$\sigma_{exc} = K\frac{\sigma_{Si}N_{Si}}{k_t C_{ind}N_{Er}} + \sigma_d. \tag{7}$$

In order to properly fit the data we have considered that the σ_{exc} of Er^{3+} decays with the distance R from the Si-nc until it becomes that of the direct excitation σ_d:

$$\sigma_{exc}(R) = \sigma_0 \exp\left(-\frac{R - R_{nc}}{R_0}\right) + \sigma_d. \tag{8}$$

Here, R_{nc} is the Si-nc radius and R_0 a parameter. This is equivalent to consider a coupling rate K that decays with the distance.[23] The picture behind this model is of a system where Er^{3+} ions near the Si-nc are efficiently coupled to them, whereas Er^{3+} ions far away behave as Er^{3+} in SiO_2 (or in SiO_x according to the annealing time and to the simulations shown in Fig. 1). Those last ions can be excited only directly. The rate eq. (6) is then solved for each R as a function of the pump photon flux. Thus, by integrating over R, we get the temporal dependence of the total excited state population.

In Fig. 5, we have plotted the experimental data of the excited state population as a function of the pump flux. There are also represented the simulations of the Er^{3+} population excited through nanoclusters and directly. The superposition of these two curves reproduces quite well the experimental data. Using the same parameters, we have also reproduced the difference between the reciprocals of the rise and decay times for low Φ (inset of Fig. 5). In order to fit both the sets of data (lifetime for low pump fluxes and PL measurements for higher fluxes) we had to assume that only 2–3% of the total Er^{3+} population is coupled to the Si-nc, that the typical interaction distance is $R_0 \sim 0.5$ nm and that σ_0 is $\sim 10^{-16}$ cm^2. These numbers mean that a large volume percentage of the material is indeed occupied by Er^{3+} ions that are too far from a Si-nc and, thus, they are not able to be excited through indirect transfer but through direct photon absorption. The low percentage of Er^{3+} excitable through the Si-nc is the most pressing issue for the moment as it hugely reduces the possible performances of the material as an active material.

Equation (8) explains also the observation of Fig. 4: as one increases Φ, the Er^{3+} coupled to Si-nc are saturated and the excitation of more distant Er^{3+} ions is now occurring directly which translates into a decrease of σ_{exc}. Saturation is due to the ms lifetime of Er^{3+} compared to the μs transfer time from Si-nc to Er^{3+}. A detailed modeling addressing this problem is the subject of another letter.[23] It is also worth noting that a combination of this model together with a flux dependent coupling constant (due to excited state absorption or Auger back transfer) can also lead to a good reproducibility of the experimental results.

6. Signal Enhancement

Since we are interested in a waveguide amplifier, we performed amplification studies. What we measured is the signal enhancement factor SE, which is equal to the ratio of the transmitted signal intensity when the waveguide is excited, i.e., under pumping I_{PP}, to the transmitted signal intensity when the waveguide is not excited, i.e., without pump (I_P). To model $SE = I_{PP}/I_P$, we approximate the system as a two level system and we work in the regime of weak probes,[34] then

$$\begin{aligned}SE &= \exp(2\sigma_{em}N_2\Gamma L) \\ &\approx \exp\left[\left(\frac{2\Phi\sigma_{exc}}{\frac{1}{\tau_d(\Phi)} + \Phi\sigma_{exc}}\right)\sigma_{em}N_{Er}L\Gamma\right],\end{aligned} \tag{9}$$

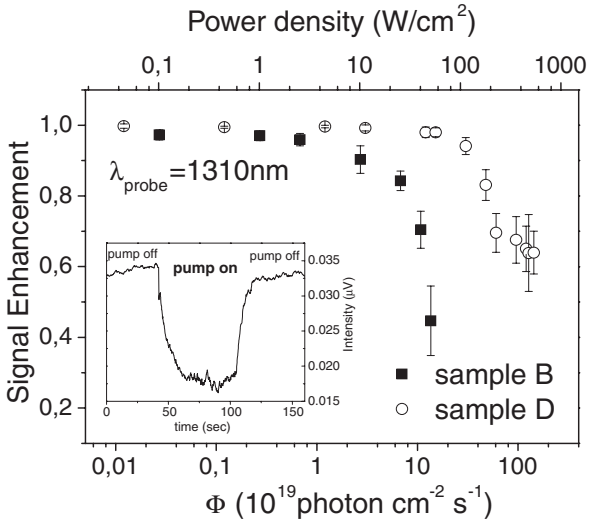

Fig. 6. Signal enhancement as a function of pump photon fluxes (wavelength 532 nm) when using a 1310 nm wavelength probe signal. The inset of the figure shows the time variation of the probe signal when the pump is switched off and on.

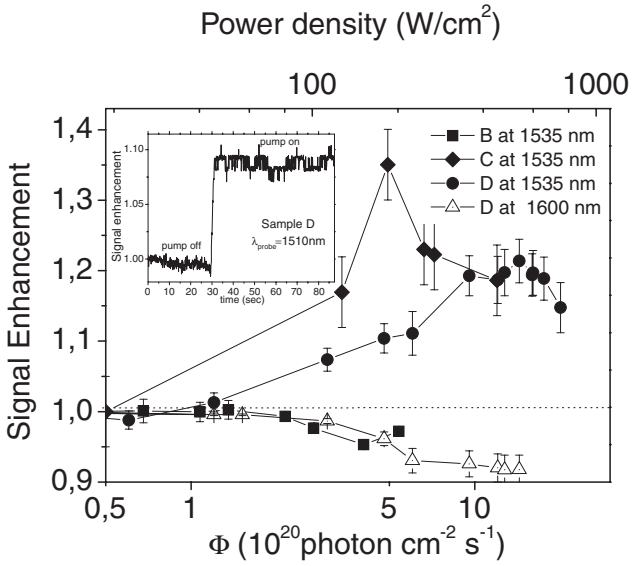

Fig. 7. Signal enhancement using a 1535 nm wavelength probe signal for samples B (squares), C (diamonds), and D (circles). Empty triangles are the signal enhancement at a probe wavelength of 1600 nm. The pump wavelength was 532 nm for samples B and D and 488 nm for sample C. The inset shows the time variation of the probe signal when the pump is switched off and on.

where L is the length of the excited volume. The Φ dependence of τ_d was already explained in the previous section mainly in terms of cooperative up-conversion mechanisms. It is also worth noting that the internal gain coefficient in cm^{-1} will be defined as $g = \sigma_{em} N_2 \Gamma$.

Figure 6 reports the signal enhancement at a wavelength of 1310 nm as a function of Φ. Er^{3+} does not have any absorption resonance at this wavelength. Thus, the decreasing SE is due to a flux-dependent propagation loss mechanism. The most suitable candidate is confined CA within the Si-nc: an absorption mechanism, which depletes the Si-nc excited population and, as a consequence, introduces a new loss mechanism for the signal light and turns off the excitation of Er^{3+} via Si-nc.[13] When decreasing the annealing time, this detrimental CA process is decreased. In fact, $SE = 0.7$ for $\Phi = 1 \times 10^{20}$ photons $cm^{-2}\,s^{-1}$ for sample B while $SE = 0.7$ for $\Phi = 6 \times 10^{20}$ photons $cm^{-2}\,s^{-1}$ for sample D. Sample C showed a similar behavior to what observed in sample D. In ref. 13, we used a resonant pump wavelength of 488 nm, and found a lower CA contribution. These two experimental evidences support the attribution of the Φ-dependent losses to CA. Indeed CA decreases when the Si-nc sizes decreases and CA increases quadratically with Φ. The inset of Fig. 6 shows the time dependence of SE: it has long turn-on and turn-off times. These long times cannot be explained by the lifetime of excitons in Si-nc, which are of the order of tens of microseconds. As suggested in ref. 8, these long lifetimes can be attributed to excitons, which are formed by electrons and holes excited in nearby Si-nc and thus separated by a large distance. It has been recently observed by Forcales *et al.*[24] similar long lifetime behaviors on ion implanted samples, explained in terms of the presence of specific charge traps within nanoclusters or damaged nanocrystals.

When using a signal wavelength of 1535 nm, we are probing the Er^{3+} absorption band maximum. Figure 7 shows the measured SE as a function of Φ while the inset of the figure shows the temporal behavior of the probe when the pump is switched on. SE for sample B is weakly below 1: pump induced absorption is present. However, as we increase the pump rate a weak increase of SE is observed. This behavior has been already discussed in ref. 13 as due to two competing mechanisms: CA in the Si-nc and amplification due to direct pumping of the Er^{3+} ions. Instead, in samples C and D, $SE > 1$ and reaches a maximum of 1.35 (0.65 dB/cm) and 1.22 (0.43 dB/cm) respectively at a power density of few hundreds of W cm^{-2}. This internal gain is due to indirect excited Er^{3+}. For higher pump power, two competing mechanisms act on the Si-nc: energy transfer to the Er^{3+} and CA. Let us concentrate on CA. Once a Si-nc is excited, it is prone to absorb a signal photon. This process on one side increases the losses at the signal photon wavelength, on the other side depletes the Si-nc excitation. As a consequence, the effective excitation cross section of Er^{3+} decreases and the propagation losses at the signal wavelength increase. This is what one can readily see in Fig. 7: at high Φ, SE decreases in both samples. Note that in ref. 13 for sample B we were able to achieve a maximum $SE =$ 1.06 (0.12 dB/cm) at one order of magnitude higher photon flux while pumping at 488 nm, i.e., resonantly with an Er^{3+} absorption band.

A rough data analysis allows correcting the SE data from the CA losses; we have divided the SE data at 1535 nm by the SE measured at 1600 nm, where the emission of Er^{3+} is quite low. As a result, we obtain a maximum SE of 1.42 (1.52 dB/cm) and 1.30 (1.12 dB/cm) for samples C and D respectively, that translates in an internal gain of 0.76 dB/cm (0.18 cm^{-1}) at $\Phi = 5 \times 10^{20}$ photon $cm^{-2}\,s^{-1}$ for sample C and 0.56 dB/cm (0.13 cm^{-1}) at $\Phi = 1 \times 10^{21}$ photon $cm^{-2}\,s^{-1}$ for sample D. These values are significantly higher than the 0.2 dB/cm found in sample B at similar Φ.[13] It has also to be noted that in sample B it is possible to achieve an internal gain of 0.6 dB/cm (comparable to the other samples) at a higher Φ of about 10^{22} photon $cm^{-2}\,s^{-1}$.

Since $g = \sigma_{em} N_2 \Gamma$ and the absorption coefficient $\alpha = \sigma_{abs} N_{Er} \Gamma$, then

$$\frac{g}{\alpha} = \frac{\sigma_{em} N_2}{\sigma_{abs} N_{Er}} \approx \frac{N_2}{N_{Er}} \tag{10}$$

by assuming that at 1535 nm $\sigma_{em} = \sigma_{abs}$.[26] Thus, we can estimate the percentage of Er^{3+} ions in the excited state. It results about 11, 9, and 7% of the total active erbium population for samples B, C, and D, respectively. These low inversion fractions are mainly due to a low population of Er^{3+} ions coupled to Si-nc, actually less than 3% of the Er content is coupled to Si-nc in these samples,[23] being the rest excitable only through direct pumping.

Quantitative measurements of the photon flux emitted from these samples have allowed us to determine the number of Er^{3+} ions that are emitting as a function of Φ.[28] For example, in sample B, at emission saturation (high pumping Φ), $N_2 \cong 3 \times 10^{19}$ ions cm^{-3}. From eq. (10), we found that $N_2/N_{Er} = 11\%$, thus it results that $N_{Er} \cong 3 \times 10^{20}$ ions cm^{-3}, which fits quite well with the Er content determined by RBS (about 4×10^{20} ions cm^{-3}). This evidences that all the Er deposited in the sample is optically active.

The partial inversion of Er^{3+} is confirmed also by the spectral dependence of SE. Figure 8 reports the data of sample D at $\Phi = 1 \times 10^{21}$ photon cm^{-2} s^{-1} as a function of the probe wavelength. As it was observed for EDFA, partial inversion is observed as a signal enhancement which is larger than 1 at short wavelengths and smaller than 1 at longer wavelengths.[33] In addition, the spectrum is distorted by the CA losses which depend quadratically on the wavelength as it is well established for bulk silicon,[35,36] i.e., CA reduces more the probe photon flux for longer wavelengths.

It is interesting to compare the σ_{exc} measured at low Φ (Fig. 4) with those extracted from the SE at high Φ. Considering that all Er^{3+} ions are optically active as previously demonstrated, and using the approximation $1/\tau_d(\Phi) = 1/\tau_d(\Phi \approx 0) + C_{up} N_2(\Phi, t = 0)$ to account for cooperative up-conversion, eq. (9) for samples C and D yields $\sigma_{exc} \cong 6 \times 10^{-20}$ cm^2 at $\Phi = 1.4 \times 10^{21}$ photon cm^{-2} s^{-1} and $\sigma_{exc} = 1 \times 10^{-20}$ cm^2 for sample B at a similar photon flux

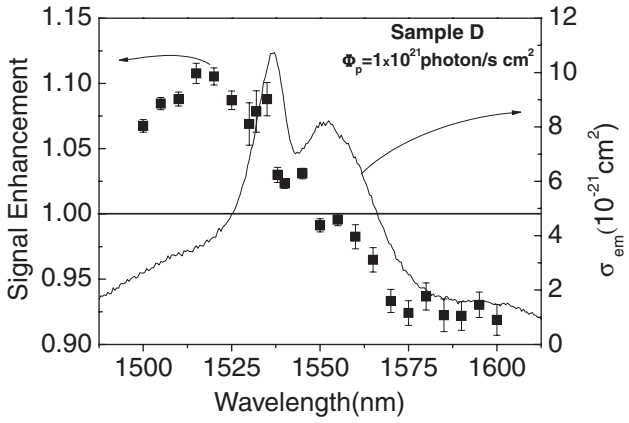

Fig. 8. Mean value of the signal enhancement (points) for different probe wavelengths at a fixed pump flux of 1×10^{21} photon cm^{-2} s^{-1}. The pump wavelength was 532 nm. The line refers to the emission cross section spectrum.

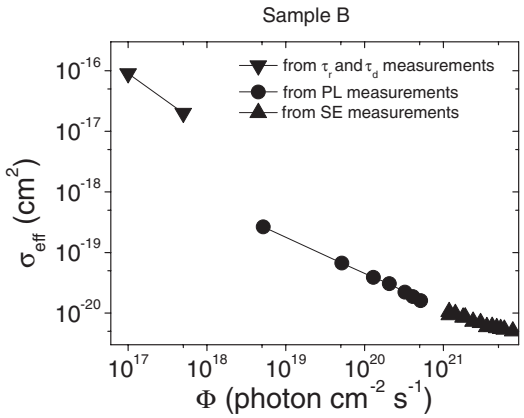

Fig. 9. Effective excitation cross-section of Er^{3+} as a function of the incident flux extracted from lifetime measurements (inverted triangles), from quantitative measurements of the density of excited Er^{3+} ions (circles) and from SE measurements (triangles). The pump wavelength is 488 nm, while the probe wavelength in the region of high pump photon flux was 1535 nm.

density. These values are similar to σ_{abs} for direct excitation of Er^{3+}, which means that most of the erbium is excited at high Φ by direct internal absorption. Sample B shows lower σ_{exc} than the other two samples that show similar values. Several causes are responsible for this: CA turns off the excitation of Er^{3+} via Si-nc in a stronger way for sample B than for the others, as it was shown in Fig. 6; in addition, the absorption cross section is smaller in sample B than in the others (Fig. 2 and ref. 18). At low Φ we are measuring orders of magnitude higher effective cross sections because most of the PL signal is coming from Er^{3+} excited via transfer from the Si-nc, as previously discussed.

Figure 9 reports the σ_{exc} obtained from SE data as a function of Φ for sample B. σ_{exc} values for low Φ (10^{17} photon cm^{-2} s^{-1}) are extracted from lifetime measurements, for intermediate Φ (10^{18}–10^{20} photon cm^{-2} s^{-1}) from quantitative measurements of the absolute amount of excited Er^{3+}, and for high Φ (10^{21}–10^{22} photon cm^{-2} s^{-1}) from SE measurements. The main result is that σ_{exc} decreases with Φ several orders of magnitude in the range of studied pump photon fluxes. This trend is compatible to what shown in Fig. 4 for low Φ. The σ_{exc} reduction is due to the cumulative effects of an Er^{3+}–Si-nc distance dependence and of a reduction of the transfer rate from the Si-nc to Er^{3+} because of confined carrier absorption.

7. Conclusions

We have demonstrated that a reduction of the annealing time, while keeping constant all the other processing parameters, has significantly improved the Si-nc and Er^{3+} system by reducing the contribution of confined carrier absorption at high pump powers and increasing the emission cross section. This leads to a higher signal enhancement for lower pumping rate, which is a preferred result for application of the system in waveguide amplifiers. The reduced annealing time affects mainly the quality of the silica matrix in terms of reconstruction of the network yielding defected silica in which small Si-nc form. A larger up-conversion coefficient has been also observed for the short annealed samples, which translates into a shorter Er^{3+}

lifetime. In this respect, a matrix of poor quality seems to favor the dimerization of the Er^{3+} ions and hence the phenomenon of up-conversion.

In any case, the main problem limiting the achievement of a net overall gain in the waveguide amplifier is lying in the few percentage of the erbium population that can be excited through the Si-nc and, hence, restricting the advantage of the properties of the coupled system. In addition, a flux dependent effective excitation cross section has been demonstrated due to the distance dependent coupling coefficient. Higher flux yields lower excitation cross section due to the saturation of the strongly coupled ions. Thus, the main problem to obtain overall gain with this system concerns the nanoengineering of the material composition allowing the production of materials with a high density of small sized Si-nc coupled effectively to all the Er^{3+} in the system. The small size is needed to minimize the CA, while the high density is necessary to increase the coupling with Er^{3+}.

Acknowledgements

This work is supported by EC through the projects SINERGIA (FP5-29650) and LANCER (FP6-033574). We thank G. Pucker of FBK-irst for the rib waveguide processing and C. Sada for material assessment. We kindly acknowledge C. Dufour for fruitful discussion.

1) A. J. Kenyon, P. F. Trwoga, M. Federighi, and C. W. Pitt: J. Phys.: Condens. Matter **6** (1994) L319.
2) M. Fujii, M. Yoshida, Y. Kanzawa, S. Hayashi, and K. Yamamoto: Appl. Phys. Lett. **71** (1997) 1198.
3) G. Franzò, V. Vinciguerra, and F. Priolo: Appl. Phys. A **69** (1999) 3.
4) J. H. Shin, S.-Y. Seo, S. Kim, and S. G. Bishop: Appl. Phys. Lett. **76** (2000) 1999.
5) P. G. Kik, M. L. Brongersma, and A. Polman: Appl. Phys. Lett. **76** (2000) 2325.
6) F. Priolo, G. Franzò, D. Pacifici, V. Vinciguerra, F. Iacona, and A. Irrera: J. Appl. Phys. **89** (2001) 264.
7) D. Pacifici, G. Franzò, F. Priolo, F. Iacona, and L. Dal Negro: Phys. Rev. B **67** (2003) 245301.
8) P. G. Kik and A. Polman: in *Towards the First Silicon Laser*, ed. L. Pavesi *et al.* (Kluwer, Dordrecht, 2003) NATO Science Series II, Vol. 93, p. 383.
9) F. Iacona, D. Pacifici, A. Irrera, M. Miritello, G. Franzò, and F. Priolo: Appl. Phys. Lett. **81** (2002) 3242.
10) M. Perálvarez, C. García, M. López, B. Garrido, J. Barreto, C. Domínguez, and J. A. Rodríguez: Appl. Phys. Lett. **89** (2006) 051112.
11) J. H. Shin, H. S. Han, and S. Y. Seo: in *Towards the First Silicon Laser*, ed. L. Pavesi *et al.* (Kluwer, Dordrecht, 2003) NATO Science Series II, Vol. 93, p. 401.
12) J. Lee, J. H. Shin, and N. Park: J. Lightwave Technol. **23** (2005) 19.
13) N. Daldosso, D. Navarro-Urrios, M. Melchiorri, L. Pavesi, F. Gourbilleau, M. Carrada, R. Rizk, C. García, P. Pellegrino, B. Garrido, and L. Cognolato: Appl. Phys. Lett. **86** (2005) 261103.
14) P. G. Kik and A. Polman: J. Appl. Phys. **91** (2002) 534.
15) W. H. Loh and A. J. Kenyon: IEEE Photonics Technol. Lett. **18** (2006) 289.
16) C. J. Oton, W. H. Loh, and A. J. Kenyon: Appl. Phys. Lett. **89** (2006) 031116.
17) P. Pellegrino, B. Garrido, J. Arbiol, C. Garcia, Y. Lebour, and J. R. Morante: Appl. Phys. Lett. **88** (2006) 121915.
18) F. Gourbilleau, C. Dufour, M. Levalois, J. Vicens, R. Rizk, C. Sada, F. Enrichi, and G. Battaglin: J. Appl. Phys. **94** (2003) 3869.
19) F. Gourbilleau, M. Levalois, C. Dufour, J. Vicens, and A. Rizk: J. Appl. Phys. **95** (2004) 3717.
20) M. Fujii, K. Imakita, K. Watanabe, and S. Hayashi: J. Appl. Phys. **95** (2004) 272.
21) P. K. Tien: Appl. Opt. **10** (1971) 2395.
22) D. Navarro-Urrios, M. Melchiorri, N. Daldosso, L. Pavesi, C. García, P. Pellegrino, B. Garrido, G. Pucker, F. Gourbilleau, and R. Rizk: J. Lumin. **121** (2006) 249.
23) B. Garrido, C. García, P. Pellegrino, D. Navarro-Urrios, N. Daldosso, L. Pavesi, F. Gourbilleau, and R. Rizk: Appl. Phys. Lett. **89** (2006) 163103.
24) M. Forcales, N. J. Smith, and R. G. Elliman: J. Appl. Phys. **100** (2006) 014902.
25) N. Daldosso, D. Navarro-Urrios, M. Melchiorri, L. Pavesi, C. Sada, F. Gourbilleau, and R. Rizk: Appl. Phys. Lett. **88** (2006) 161901.
26) W. J. Miniscalco and R. S. Quimby: Opt. Lett. **16** (1991) 258.
27) N. Daldosso, M. Melchiorri, F. Riboli, M. Girardini, G. Pucker, M. Crivellari, P. Bellutti, A. Lui, and L. Pavesi: J. Lightwave Technol. **22** (2004) 1734.
28) N. Daldosso, D. Navarro-Urrios, M. Melchiorri, C. García, P. Pellegrino, B. Garrido, C. Sada, G. Battaglin, F. Gourbilleau, R. Rizk, and L. Pavesi: IEEE J. Sel. Top. Quantum Electron. **12** (2006) 1607.
29) E. Snoeks, A. Lagendijk, and A. Polman: Phys. Rev. Lett. **74** (1995) 2459.
30) D. Kovalev, J. Diener, H. Heckler, G. Polisski, N. Künzner, and F. Koch: Phys. Rev. B **61** (2000) 4485.
31) A. J. Kenyon, C. E. Chryssou, C. W. Pitt, T. Shimizu-Iwayama, D. E. Hole, N. Sharma, and C. J. Humphreys: J. Appl. Phys. **91** (2002) 367.
32) S. Seo and J. H. Shin: Appl. Phys. Lett. **75** (1999) 4070.
33) P. C. Becker, N. A. Olsson, and J. R. Simpson: *Erbium-Doped Fiber Amplifiers* (Academic, New York, 1999).
34) H. S. Han, S. Y. Seo, and J. H. Shin: Appl. Phys. Lett. **79** (2001) 4568.
35) W. Spitzer and H. Y. Fan: Phys. Rev. **108** (1957) 268.
36) P. E. Schmid: Phys. Rev. B **23** (1981) 5531.